JCTC Journal of Chemical Theory and Computation

Constrained Density Functional Theory and Its Application in Long-Range Electron Transfer

Qin Wu* and Troy Van Voorhis

Department of Chemistry, Massachusetts Institute of Technology, Cambridge, Massachusetts 02139

Received December 9, 2005

Abstract: Recently, we have proposed an efficient method in the Kohn−Sham density functional theory (DFT) to study systems with a constraint on their density (*Phys. Rev. A* **2005**, *72*, 24502). In our approach, the constrained state is calculated directly by running a fast optimization of the constraining potential at each iteration of the usual self-consistent-field procedure. Here, we show that the same constrained DFT approach applies to systems with multiple constraints on the density. To illustrate the utility of this approach, we focus on the study of long-range charge-transfer (CT) states. We show that constrained DFT is size-consistent: one obtains the correct long-range CT energy when the donor−acceptor separation distance goes to infinity. For large finite distances, constrained DFT also correctly describes the $1/R$ dependence of the CT energy on the donor−acceptor separation. We also study a model donor−(amidinium−carboxylate)−acceptor complex, where experiments suggest a proton-coupled electron-transfer process. Constrained DFT is used to explicitly calculate the potential-energy curves of both the donor state and the acceptor state. With an appropriate model, we obtain qualitative agreement with experiments and estimate the reaction barrier height to be 7 kcal/mol.

1. Introduction

Density functional theory (DFT) as in the framework of Hohenberg, Kohn, and Sham[1,2] is a ground-state theory because there is a one-to-one mapping between the ground-state density and the external potential. Time-dependent DFT (TDDFT) is based on the analogous mapping between the time-dependent density and external potential[3] and is an extremely useful tool for calculating excitation energies through the linear response of the ground-state density.[4,5] TDDFT, in principle, exactly produces the whole electronic spectrum. In practice, even with the seemingly crude adiabatic local density approximation (ALDA) where the ground-state time-independent exchange correlation functional is used in place of the time-dependent exchange correlation action, TDDFT calculations give excitation energies of low-lying states that agree well with experiments.[6,7] However, there are also a few well-known failures of ALDA and the approximate ground-state functional employed in TDDFT. For example, Rydberg states can only be correctly described by TDDFT after an asymptotic correction to the ground-state Kohn−Sham (KS) potential.[8−10] Here, the exchange correlation potential is forced to decay as $-1/r$ asymptotically with r being the distance from the nuclei. Recent studies also indicate the importance of the intermediate part of the exchange correlation potential.[11,12] Another failure of ALDA is that excitation energies of long-range charge-transfer (CT) states are seriously in error because of the local approximation in the exchange correlation kernel.[13−15] Long-range charge transfer is a key energy-transfer step in biological photosynthetic complexes,[16] dye-sensitized solar cells,[17] and organic light emitting diodes.[18] The failure of TDDFT for CT states puts its application to these systems in jeopardy. Therefore, much effort has been spent to explore the origin of the failure, and corrections have been proposed.[19−24] The origin of the failure has been linked to the derivative discontinuity of the exchange correlation potential[25] as well as self-interaction error. The energy of a long-range CT excitation can be approximated as the energy required to remove an electron from the electron donor, that is, the ionization potential (IP) of the

* Corresponding author fax: 617-253-7030; e-mail: qinwu@mit.edu.

10.1021/ct0503163 CCC: $33.50
Published on Web 03/15/2006

donor, minus the energy gain of putting the electron to the acceptor, that is, the electron affinity (EA) of the acceptor, plus a correction of the Coulomb interaction (cf. section 3.1 below). However, in DFT, though the highest occupied molecular orbital (HOMO) energy is the IP, the energy of the lowest unoccupied molecular orbital (LUMO) cannot be associated with EA because of the derivative discontinuity.[25] ALDA, on the other hand, gives a long-range CT excitation energy that is simply the energy difference between the HOMO of the donor and the LUMO of the acceptor because the kernel is local and provides no correction for long-range Coulomb interactions between the particle and hole. Thus, the ALDA excitation energies of long-range CT states are not reliable.

Recently, we have shown[26] that long-range CT states can be accurately captured through a constrained DFT method.[27] Constrained DFT is based on time-independent ground-state DFT. It focuses on a system whose ground-state density is required to satisfy some specific constraint. With the Lagrange multiplier approach, a constraining potential is introduced to enforce the desired density constraint. The key observation we make is that any excited state that has a qualitatively different density from the ground state can be obtained using constrained DFT. For instance, in a system consisting of an electron donor (D) and an electron acceptor (A), the ground state might have both the donor and acceptor being neutral (DA). In many applications, one is interested in the particular CT excited state that has a positive charge on the donor and a negative charge on the acceptor (D^+A^-). One can obtain this low-energy CT state by minimizing the total energy under an explicit constraint that the electron density has to correspond to D^+A^-. Because constrained DFT calculates the CT state directly rather than as a time-dependent response of the ground state, it avoids the problems associated with the exchange correlation kernel in ALDA. Therefore, constrained DFT gives good results for long-range CT state energies.[26]

Constrained optimization is, of course, not new to DFT. There is a basic constraint that has to be satisfied by all DFT methods when they minimize the energy: the electron density integrates to give the total number of electrons. The important quantity associated with this constraint is chemical potential (for a detailed discussion of chemical potential, see ref 28). In the Kohn−Sham formalism of DFT, where the lowest-energy orbitals of a noninteracting system are used to construct the electron density, the chemical potential can be chosen as any value between the energy levels of HOMO and LUMO. However, the constraining potentials associated with other constraints such as those for the CT states are not so obvious to determine. Therefore, most applications of constrained DFT rely on scanning over various potentials to find the one that meets the target criterion.[27,29−31] This is equivalent to applying various perturbations to the ground state and so is also referred to as the "perturbed ground state" method.[32] Recently, we have developed a direct optimization method to calculate the constraining potential.[26] Our method starts from the usual Lagrange multiplier approach for constrained optimization problems. However, instead of treating the constraining potential and orbitals as independent variables, we make use of the stationary equations for the orbitals and the technique of optimized effective potential[33,34] to transform the energy functional into a concave function of the constraining potential only.[35] The maximum then exactly corresponds to the target state. Because both the first and second derivatives are easily calculated, the optimization is very efficient. Also, our method yields the target state with one self-consistent field (SCF) calculation, which is computationally much less intensive compared to the scanning method. We have shown that constrained DFT gives very good results for long-range CT states:[26] the excitation energy is accurate and displays a negative inverse dependence on the donor−acceptor distance as it should. Recently, there have been suggestions of doing constrained calculations with wave-function-based methods.[36,37] We look forward to more exciting results in that aspect also.

In this report, we present the direct optimization method to handle systems with multiple constraints. Details of our implementation are described, such as the direct inverse of iterative subspace (DIIS) approach used in assisting SCF convergence and a comparison of different electron population schemes. We then test the method with calculations of infinitely separated CT states as well as a model system for proton-coupled electron transfer. Finally, we make a connection between constrained DFT and the Marcus theory of electron transfer[38,39] and briefly discuss possible applications.

2. Method

2.1. Constrained DFT with Multiple Constraints. Suppose there are m constraints that one wants to impose on the electron density, and the kth constraint can be written, in general, as

$$\sum_{\sigma} \int w_k^{\sigma}(\mathbf{r})\, \rho_{\sigma}(\mathbf{r})\, \mathrm{d}\mathbf{r} - N_k = 0 \tag{1}$$

where σ stands for either α or β spin, w_k is the weight function that defines the constrained property, and N_k is the constraint value. ρ_σ is calculated as $\sum_i^{N_\sigma} |\phi_{i\sigma}(\mathbf{r})|^2$ in the KS scheme, with $\phi_{i\sigma}$ being the ith lowest energy orbital and N_σ the number of σ electrons. The sum of ρ_α and ρ_β gives the total electron density ρ. Our goal is to minimize the electronic energy, a functional of ρ, under all constraints in eq 1. Creating a Lagrange multiplier, V_k, for each constraint and adding every product of the corresponding multiplier and constraint to the energy functional forms a new functional:

$$W[\rho,\{V_k\}] = E[\rho] + \sum_k^m V_k\Big[\sum_{\sigma} \int w_k^{\sigma}(\mathbf{r})\, \rho_{\sigma}(\mathbf{r})\, \mathrm{d}\mathbf{r} - N_k\Big] \tag{2}$$

$E[\rho]$ in the KS scheme is calculated by

$$E[\rho] = \sum_{\sigma}\sum_{i}^{N_\sigma} \left\langle \phi_{i\sigma} \middle| -\frac{1}{2}\nabla^2 \middle| \phi_{i\sigma} \right\rangle + \int \mathrm{d}\mathbf{r}\, v_n(\mathbf{r})\, \rho(\mathbf{r}) + J[\rho] + E_{\mathrm{xc}}[\rho^{\alpha},\rho^{\beta}] \tag{3}$$

where J is the classical Coulomb energy, E_{xc} is the exchange correlation energy, and v_n is the external potential. The

stationary equations of W with respect to the orbitals, which are required to be normalized, then are

$$\left[-\frac{1}{2}\nabla^2 + v_n(\mathbf{r}) + \int \frac{\rho(\mathbf{r}')}{|\mathbf{r}-\mathbf{r}'|}\,d\mathbf{r}' + v_{xc\sigma}(\mathbf{r}) + \sum_k^m V_k\, w_k^\sigma(\mathbf{r})\right]\phi_{i\sigma} = \epsilon_{i\sigma}\phi_{i\sigma} \quad (4)$$

with a similar one for $\phi_{i\sigma}^*$. These are the standard KS equations except for the addition of constraining potentials, $\sum_k^m V_k\, w_k^\sigma(\mathbf{r})$, in the effective Hamiltonian. Equation 4 is solved together with eq 1 to yield V_k and ϕ_i. In the following, when there is no confusion, we simply use V_c to represent the set of $\{V_k\}$, where $k = 1, ..., m$, and the same applies to N_c and w_c.

Because, for any given V_c, eq 4 uniquely determines a set of orbitals, if only the orbitals from eq 4 are to be explored, W becomes a function of V_c only. Furthermore, $W(V_c)$ is a concave function of V_c as we now show. Following ref 35, the first derivatives of $W(V_c)$ are

$$\frac{\partial W}{\partial V_k} = \sum_\sigma \sum_i^{N_\sigma} \left(\frac{\delta W}{\delta \phi_{i\sigma}^*}\frac{\partial \phi_{i\sigma}^*}{\partial V_k} + \text{cc}\right) + \frac{\partial W}{\partial V_k} = \sum_\sigma \int w_k^\sigma(\mathbf{r})\,\rho_\sigma(\mathbf{r})\,d\mathbf{r} - N_k \quad (5)$$

Here, the fact that $\delta W/\delta\phi_{i\sigma}^* = 0$, that is, eq 4, has been used. The stationary point of $W(V_c)$, which means $\partial W/\partial V_k = 0$, then restores the constraints of eq 1 automatically. It remains to show that the second derivative matrix (Hessian) of $W(V_c)$ is nonpositive definite to prove that $W(V_c)$ is concave. Starting from eq 5,

$$\frac{\partial^2 W}{\partial V_k \partial V_l} = \sum_\sigma \sum_i^{N_\sigma} \int w_k^\sigma(\mathbf{r})\,\phi_{i\sigma}^*(\mathbf{r}) \frac{\delta \phi_{i\sigma}(\mathbf{r})}{\delta[V_l\, w_l^\sigma(\mathbf{r}')]} w_l^\sigma(\mathbf{r}')\,d\mathbf{r}\,d\mathbf{r}' + \text{cc}$$

$$= \sum_\sigma \sum_i^{N_\sigma} \int w_k^\sigma(\mathbf{r})\,\phi_{i\sigma}^*(\mathbf{r}) \sum_{a\neq i} \frac{\phi_{a\sigma}^*(\mathbf{r}')\,\phi_{i\sigma}(\mathbf{r}'')}{\epsilon_{i\sigma}-\epsilon_{a\sigma}} \phi_{a\sigma}(\mathbf{r})\, w_l^\sigma(\mathbf{r}')\,d\mathbf{r}\,d\mathbf{r}' + \text{cc}$$

$$= 2\sum_\sigma \sum_i^{N_\sigma} \sum_{a>N_\sigma} \frac{\langle\phi_{i\sigma}|w_k^\sigma|\phi_{a\sigma}\rangle\langle\phi_{i\sigma}|w_l^\sigma|\phi_{a\sigma}\rangle}{\epsilon_{i\sigma}-\epsilon_{a\sigma}} \quad (6)$$

Here, the first-order perturbation theory is used to evaluate $\delta\phi_{i\sigma}(\mathbf{r})/\delta[V_l\, w_l^\sigma(\mathbf{r}')]$. In the final expression, the index i goes over occupied orbitals, while a only has to go over the unoccupied orbitals because the summand is antisymmetric with the exchange of i and a. The Hessian is nonpositive definite because, for any V_c,

$$\sum_{k,l}^m V_k \frac{\partial^2 W}{\partial V_k \partial V_l} V_l = 2\sum_\sigma \sum_i^{N_\sigma} \sum_{a>N_\sigma} \frac{\langle\phi_{i\sigma}|\sum_k^m V_k\, w_k^\sigma|\phi_{a\sigma}\rangle^2}{\epsilon_{i\sigma}-\epsilon_{a\sigma}} \le 0 \quad (7)$$

This is true because in the KS scheme the occupied orbitals are chosen as the lowest eigenstates; hence, $\epsilon_{i\sigma} - \epsilon_{a\sigma} < 0$, while the numerator is non-negative. This implies that there is only one stationary point of $W(V_c)$ and that it is a maximum. Thus, by optimizing W through varying V_c, one can find the constraining potential that exactly yields the ground state of the constrained system. Because both the first and second derivatives are easily calculated, the optimization can be done efficiently.

To study charge-transfer states, which are the focus of this work, one can put two separate constraints simultaneously on the donor and acceptor charges. Alternatively, one can impose just one constraint on the charge difference between the donor and the acceptor; that is, $N_c = (N_D - N_A)/2$, where N_D and N_A are the net charges on D and A.[26] This can be done by defining the weight function in eq 1 to be positive on the donor and negative on the acceptor, which effectively constrains both the donor and the acceptor, and should give the same result for the charge-separated state as that using two constraints. Therefore, in what follows, we choose to use one constraint for simplicity.

2.2. Convergence. We have implemented the direct optimization approach in NWChem.[40] Our method is formulated as an outer loop and an inner loop. First, to solve the KS equations, a SCF procedure is employed, wherein orbitals are iteratively improved. This constitutes the outer loop. Second, at each SCF iteration, an optimization is carried out to find the optimal V_c, which is the inner loop. For the optimization, the availability of both the first and second derivatives recommends the use of Newton's method (see, for example, ref 41), which can reduce the number of inner iterations. This is important because every trial V_c demands a matrix diagonalization to obtain the corresponding orbitals. However, because only V_c is updated and the Fock matrix is not rebuilt at each inner iteration, the inner loop is still relatively cheap, at least for atom-centered basis sets where the number of basis functions per atom is small.

DIIS is a powerful tool to assist the convergence of SCF procedures. With DIIS, the current Fock matrix at the nth iteration is replaced by a linear combination of previous Fock matrices. A detailed description of how to determine the linear coefficients is provided by Pulay.[42,43] Now that there is an extra inner loop, constrained DFT can still make use of DIIS to accelerate the outer-loop convergence. But because of changes to the KS equations in eq 4, the Fock matrix needs to be handled carefully. The way we use DIIS in our calculations can be summarized as follows: (1) Construct the current Fock matrix $\mathbf{F}$ from the current density matrix $\mathbf{P}$. (2) Use the optimal V_c from the last iteration to build the constrained Fock matrix $\mathbf{F}_c = \mathbf{F} + V_c\mathbf{w}_c$. (3) Determine the DIIS linear coefficients d^i, and replace the current Fock matrix with $\mathbf{F}^* = \sum_i^n d^i \mathbf{F}_c^i$. (4) Fix $\mathbf{F}^*$, and optimize V_c again until the constraints are satisfied. (5) Obtain the new density matrix from $\mathbf{F}^*$ and the optimized V_c. The new $\mathbf{P}$ and the optimized V_c are then fed into the next iteration, and the above steps are repeated until convergence. We find that the modified SCF procedure is as robust as that in normal DFT calculations.

2.3. Electron Population in a Molecule. For CT, the density constraints are generally expressed as constraints on the number of electrons associated with an atom (or a group

of atoms) in the molecule, that is, the electron population. There is no unambiguous way of defining an atom in a molecule; nevertheless, this concept must be defined for chemists.[44] When we calculate the electron population, we first consider the easiness of its implementation in existing DFT codes. We will further explore the optimal definition in our future work.

It is preferable to have the electron number of the constrained area calculated by $N_c = \mathrm{Tr}(\mathbf{P}\mathbf{w}_c)$, where Tr stands for the matrix trace, $\mathbf{P}$ is the density matrix, and $\mathbf{w}_c$ is a weight matrix in the basis set space defining both the constrained area, that is, the donor and acceptor groups, and the constrained property, that is, the charge difference between the donor and the acceptor. $\mathbf{w}_c$ should be formed at the beginning of a calculation and remain unchanged throughout the calculation. Below, we show how the Mulliken population, the Löwdin population, and Becke's multicenter integration scheme, all of which are readily available in most DFT codes, can be easily turned into a weight matrix.

For Mulliken populations,[45] the electron population of a group, for example, C, of atoms in a molecule is calculated as

$$N_c = \sum_{\mu \in C} (\mathbf{PS})_{\mu\mu} = \mathrm{Tr}(\mathbf{P}\mathbf{w}_c^{\mathrm{M}})$$

where $\mathbf{S}$ is the overlap matrix and the Mulliken weight matrix $\mathbf{w}_c^{\mathrm{M}}$ is

$$w_{c\mu\nu}^{\mathrm{M}} = \begin{cases} S_{\mu\nu} & \text{if } \mu \in C \text{ and } \nu \in C \\ \frac{1}{2}S_{\mu\nu} & \text{if } \mu \in C \text{ or } \nu \in C \\ 0 & \text{if } \mu \ni C \text{ and } \nu \ni C \end{cases}$$

For Löwdin populations,[46] the population of the same group of atoms is given by

$$\begin{aligned} N_c &= \sum_{\mu \in C} (\mathbf{S}^{1/2}\mathbf{P}\mathbf{S}^{1/2})_{\mu\mu} \\ &= \sum_{\mu \in C}\sum_{\nu\lambda} S_{\mu\nu}^{1/2} P_{\nu\lambda} S_{\lambda\mu}^{1/2} \\ &= \sum_{\nu\lambda} P_{\nu\lambda} \sum_{\mu \in C} S_{\lambda\mu}^{1/2} S_{\mu\nu}^{1/2} \\ &= \mathrm{Tr}(\mathbf{P}\mathbf{w}_c^{\mathrm{L}}) \end{aligned}$$

where $w_{c\lambda\nu}^{\mathrm{L}} = \sum_{\mu \in C} S_{\lambda\mu}^{1/2} S_{\mu\nu}^{1/2}$, defining the Löwdin weight matrix.

Becke's multicenter integration scheme[47] is widely used in DFT calculations. Here, the integration of the whole molecule is decomposed into single-center integrations by assigning a relative weight function $w_n(\mathbf{r})$ to each nucleus n. $w_n(\mathbf{r})$ is equal to 1 around its own nucleus and drops to 0 rapidly but continuously when in a region closer to another nucleus. Hence, these weight functions partition the molecule into fuzzy cells, and each cell can be viewed as an atom. Projecting the weight functions $w_n(\mathbf{r})$ of the atoms in C from real space to the basis set space then forms the Becke weight matrix $\mathbf{w}_c^{\mathrm{B}}$ with $w_{c\lambda\nu}^{\mathrm{B}} = \sum_{n \in C} \int \mathrm{d}\mathbf{r}\, \chi_\lambda(\mathbf{r})\, w_n(\mathbf{r})\, \chi_\nu(\mathbf{r})$.

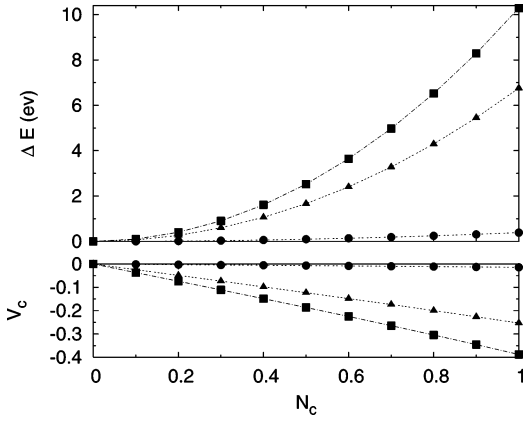

Figure 1. Energy and constraining potential as against the charge separation in N_2 with different population schemes. Squares: Becke weights population. Triangles: Löwdin population. Dots: Mulliken population. Calculations are done using Becke's three-parameter hybrid functional[48] with Lee−Yang−Parr correlation[49] and a 6-31G* basis set.

First, we compare the results of the above three population schemes. In Figure 1, the constraining potential and the increase of total energy are plotted against the amount of charge separation between the two N atoms in the N_2 molecule with a bond length of 1.12 Å. The Mulliken population apparently gives very different results from the Löwdin population and the Becke weights population. The unusually small changes in the potential and energy indicate that the results of the Mulliken population are qualitatively wrong. The reason is that the Mulliken population is not defined by a projection operator[50]—for example, a Mulliken population can be negative—therefore, Mulliken populations do not give well-defined constraints. The difference between the Löwdin population and the Becke weights population, though not small for N_2 where the two atoms are very close to each other, becomes insignificant when the donor and the acceptor are far apart. This point is well-illustrated in Figure 2, where the constraining potentials and energies of the CT states for the zincbacteriochlorin−bacteriochlorin (ZnBC−BC) complex[21] are shown. Here, $N_c = 1$ is the $\mathrm{ZnBC}^+-\mathrm{BC}^-$ state and $N_c = -1$ is the $\mathrm{ZnBC}^- - \mathrm{BC}^+$ state. Only results of the Löwdin population (black triangles) and the Becke weights population (lines) are presented, and they are nearly indistinguishable. Because the Löwdin population is easier to compute and more commonly used, it will be our first choice in all calculations. We have also tested a variant of the Löwdin population, namely, the atomic-orthogonalized Löwdin population,[51] and found the same qualitative results as those for the Löwdin population.

3. Calculations and Results

3.1. Charge-Separated States at an Infinite Distance. A good test of our method is to calculate the energy of a charge-separated (CS) state at an infinite distance, $E_{\mathrm{CS}}(\infty)$. Consider a system of an electron donor and an acceptor that are both neutral initially. The CS state is formed by transferring one electron from the donor to the acceptor. When the donor and the acceptor are far apart and there is nothing between them, one can make the valid approximation to treat both parts as point charges and obtain the relationship between

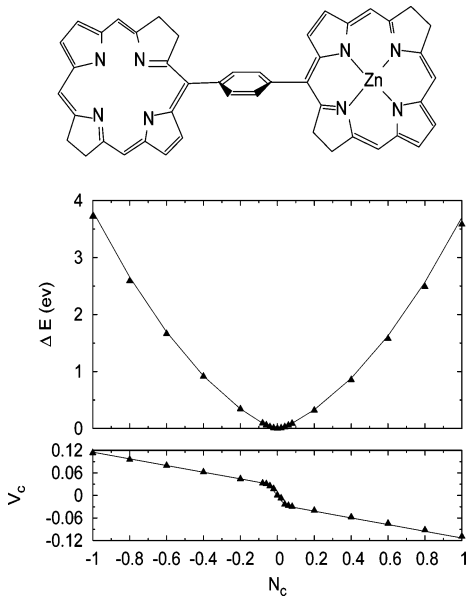

Figure 2. Energy and constraining potential as against the charge separation in the ZnBC−BC complex (shown above). Results of the Becke weights population form the line, and the black triangles are data of the Löwdin population. Calculations are done with Becke's exchange functional[52] and LYP correlation functional[49] using a 6-31G* basis set.

Table 1. Comparison of Charge-Separated State Energies with the Electron Donor (D) and Acceptor (A) Infinitely Apart and the Sum of Ionic Energies of D and A[a]

D	A	$E_D^+ + E_A^-$	$E_{CS}(\infty)$
N_2	N_2	−218.360 411	−218.361 386
H_2O	F_2	−275.391 972	−275.392 850
C_2F_4	C_2H_4	−553.595 853	−553.595 591

[a] All numbers are in hartrees.

the energy of the CS state and the separation distance (R) as In our previous report,[26] we have shown the excellent linear

$$E_{CS}(R) \approx -\frac{1}{R} + E_{CS}(\infty) \tag{8}$$

dependence of $E_{CS}(R)$ on $1/R$ given by constrained DFT. Here, we study the value $E_{CS}(\infty)$. It is evident that $E_{CS}(\infty)$ should equal the sum of individually calculated energies of D^+ and A^-. Therefore, by fitting $E_{CS}(R)$ and $1/R$ data to a straight line, the intersection parameter, which is $E_{CS}(\infty)$, should have the same value as $E_D^+ + E_A^-$.

We have tested CS state energies of three donor and acceptor molecular pairs as listed in Table 1. All calculations are done with the B3LYP functional[48,49,52] and 6-31G* basis set. Molecules are placed in two parallel planes that are perpendicular to the axis connecting their centers. The distance between the planes is defined as R, and five different R values are used, starting from $R = 8$ Å and increasing by 0.5 Å at each point. The differences between $E_{CS}(\infty)$ and $E_D^+ + E_A^-$ in all three cases are less than 1 millihartree, which are attributable to the point charge approximation and fitting errors. Thus, constrained DFT has the correct limit for a CS state. Together with the linear relationship shown in our previous work,[26] these tests demonstrate that constrained DFT is very appropriate to study long-range charge-separated states.

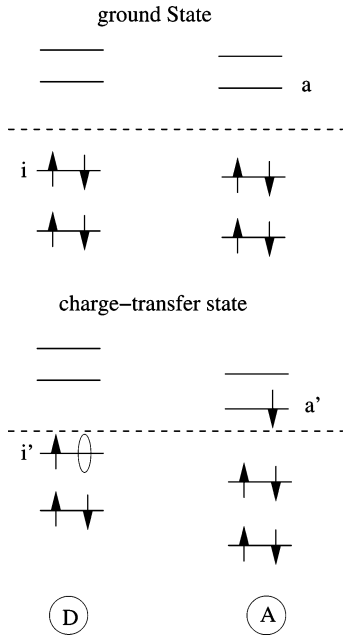

Figure 3. Illustrative picture of the frontier orbitals of the ground and CT states. The donor and acceptor molecules are far apart, so an orbital from D does not overlap with that from A. Note that orbitals *i* and *a* are different from *i′* and *a′*.

In the CS state calculations, it is important to use the unrestricted Kohn−Sham (UKS) method to break the spin symmetry because the ions are both spin-polarized and calculated with UKS. Though restricted KS (RKS) energies display a linear dependence on $1/R$ too, RKS approaches a different asymptotic value. For instance, the RKS $E_{CS}(\infty)$ for the H_2O-F_2 pair is −275.273 965 hartree, significantly higher than the unrestricted value −275.392 850 hartree.

Before we present more results, we want to explore the reason constrained DFT works for long-range CT states while TDDFT fails. Here, we follow the argument of Dreuw and Head-Gordon.[21] Figure 3 is a sketch of the frontier orbitals of the donor and acceptor molecules for the ground and CT states. Zero overlap between the orbitals of D and A is assumed. Because TDDFT uses the ground state as the reference to calculate the CT state (through linear response), it requires exact exchange to correctly account for the electron−hole Coulomb attraction, which is missing in existing pure density functionals. It also suffers from the fact that the LUMO energy in DFT cannot be connected with the electron affinity when it uses orbital *a* of the ground state for such a purpose. Constrained DFT builds the CT state directly, so the reference is not the ground state anymore, but the real CT state. Therefore, the electron−hole Coulomb interaction is calculated classically. Moreover, orbital a' of A^- is now the HOMO, which can be used as an approximation to EA of A.[53] The excitation energy of the CT state then is approximately

$$\begin{aligned}\omega_{CT} &\approx -(i'i'|a'a') - \epsilon_i + \epsilon_{a'} \\ &\approx -1/R + IP^D - EA^A \end{aligned} \tag{9}$$

which is the same formula as that used in ref 22.

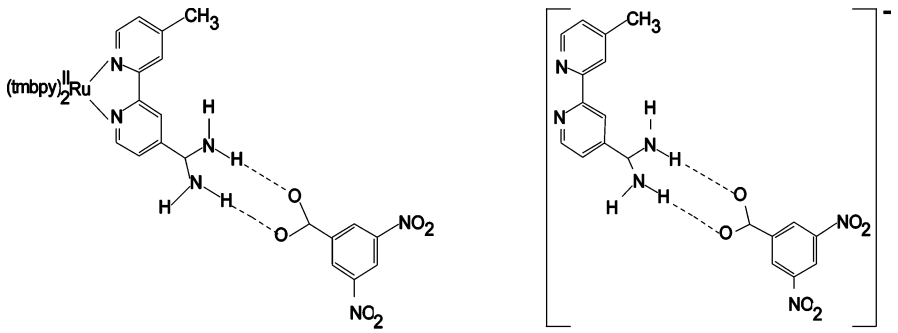

Figure 4. Real (**1**) and model systems (**2**) in studying electron transfer through hydrogen-bonded interfaces.

3.2. Electron Transfer through Hydrogen-Bonded Interfaces. Next, we study the electron transfer in a donor−(amidinium−carboxylate)−acceptor complex. Amidinium and carboxylate form a hydrogen-bonded interface that models the aspartate−arginine salt bridges in many important biological structures[54−59] and is a well-defined model for studying proton-coupled electron-transfer (PCET) reactions. Extensive studies on the kinetics of this complex have been reported experimentally and theoretically.[60−63] To predict the kinetics theoretically, it is very important to obtain the potential-energy surface for proton transfer, which can be calculated with constrained DFT.

Here, we pick the system **1**, as shown in Figure 4, for our study,[61] where tmbpy = 3,3′,4,4′-tetramethyl-2,2′-bipyridine. In this system, the electron donor is $(tmbpy)_2Ru^{II}$(Mebpy), where Mebpy = 4-methyl-2,2′-bipyridine, and the acceptor is 3,5-dinitrobenzene. As a first attempt, we optimized the geometry of **1** with the B3LYP functional and 6-31G* basis set, which is done with the Gaussian 03 program.[64] Unfortunately, one of the bridge protons moves away from the nitrogen and forms a bond with the oxygen. Thus, the structure of **1** in Figure 4 is not the most stable configuration in the gas phase, probably because the positive charge on Ru^{II} repels the bridge protons so that one of them is pushed away. What makes **1** stable in solution is solvent molecules, which are difficult to include in our calculations. Therefore, we adopt the model system **2** shown in Figure 4. The model system has an overall negative charge because an electron transfers from ruthenium to Mebpy upon excitation. However, during the excitation process, the nuclear framework should not change significantly (i.e., we make the Franck−Condon approximation). Thus, we optimize the geometry of **2** at zero charge, that is, before the electron is injected. The optimized structure agrees qualitatively with the picture in Figure 4, with both bridge protons on the nitrogen side. The N−H bond length and the N−O distance are 1.0817 and 2.6181 Å, respectively, for the upper bridge and 1.0788 and 2.6261 Å, respectively, for the lower bridge. In both bridges, the N−O distance equals the sum of N−H and O−H distances, indicating that N, H, and O can be connected by a straight line. We then fix all nuclear positions except for the upper bridge proton, which we take as the one coupled with the electron transfer. This proton is moved manually from N to O at several points along the bridge, and the energy at each point is calculated. According to B3LYP calculations, the charge is almost evenly distributed over the donor and the acceptor at all proton positions. This is because of DFT methods' artificial stabilization of systems with fractional numbers of electrons.[65,66] Hence, normal unconstrained DFT calculations cannot predict the correct electronic configuration of this molecule. Instead, energies of the states that have the charge constrained on the donor (Mebpy) or the acceptor (dinitrobenzene) are calculated at each point. With the potential-energy curves of these two states, one can then tell the preferred electronic state as the proton transfers.

We use D^-NOA and DNOA^- to denote the donor state and the acceptor state, respectively. Experimental evidence suggests that a bridge proton moves from the nitrogen side to the oxygen side as an electron transfers from the donor to the acceptor.[61] Thus, one expects the energetic picture to be that D^-NOA has a lower energy when the proton stays with the nitrogen and DNOA^- has a lower energy after the proton transfers to bond with the oxygen. Figure 5a shows the constrained B3LYP results using the 6-31G* basis set and Löwdin population. In this graph as well as in Figures 5b and 6, the (0,0) coordinate represents the state with the charge constrained on the acceptor and the proton at the equilibrium position for the neutral complex. As the position coordinate increases, the proton moves closer to the oxygen. It is clear from this graph that DNOA^- is a more stable state at all proton positions. This is contradictory to the experimental results. The calculation results do not change qualitatively when the Becke weights population is used (lines in Figure 5b). We also tested a different functional: B97-2,[67] which is reported to be better in predicting reaction barriers,[68] but the same picture is obtained (pluses in Figure 5b). Finally, we used a much larger basis set of 6-311++G**, but the DNOA^- is still much lower in energy than D^-NOA (squares in Figure 5b).

To test the reliability of DFT methods in this case, we calculated the EA of Mebpy and dinitrobenzene. We took the geometry of Mebpy and dinitrobenzene as they are in the model system, used a hydrogen to terminate each group, and then calculated the vertical EA as E(neutral) − E(anion) at the same geometry. With B3LYP and 6-31G*, the vertical EA of Mebpy is −7.9 kcal/mol, which means its anion is not stable. This result is consistent with the fact that there have been no experimental observations of the EA for this molecule. The vertical EA of *m*-dinitrobenzene is 30.2 kcal/mol, in good agreement with the experimental value 38.05 kcal/mol.[69] This result concurs with other findings that DFT generally gives a good approximation to EA.[70−72] With such

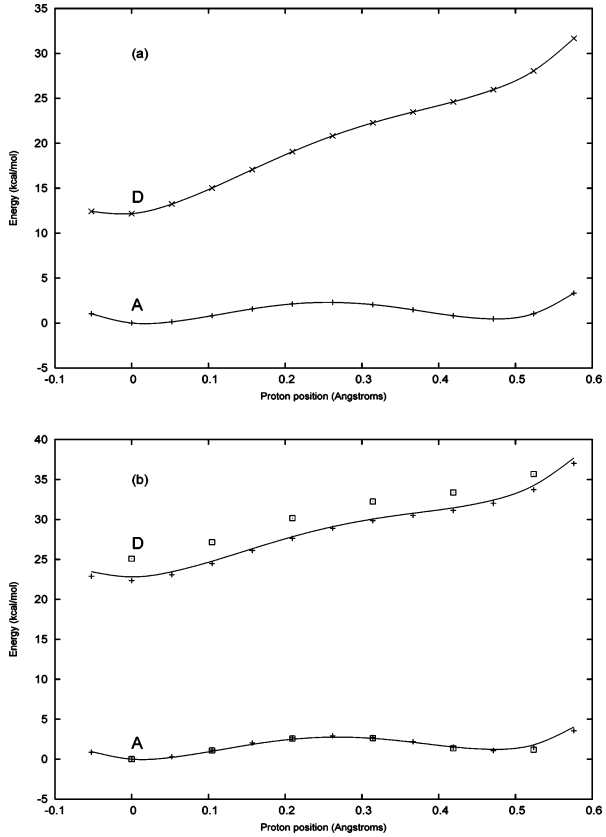

Figure 5. Constrained state energies of D^-NOA (D) and $DNOA^-$ (A) as a function of the proton position. (a) B3LYP/6-31G* and the Löwdin population. (b) Lines: B3LYP/6-31G* and Becke weights population. Crosses: B97-2/6-31G* and Becke weights population. Squares: B97-2/6-311++G** and Becke weights population.

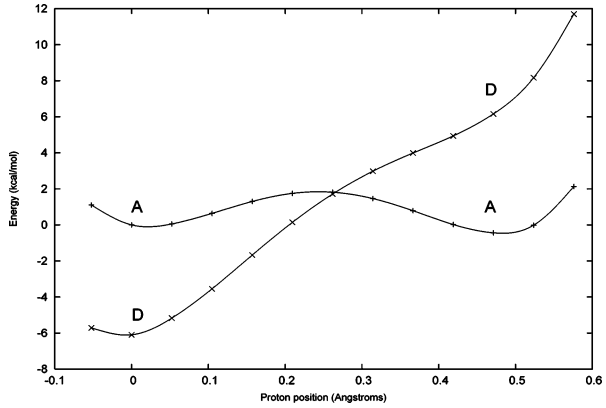

Figure 6. Constrained state energies of D^-NOA (D) and $DNOA^-$ (A) as a function of the proton position. A point charge of +0.3 is in place of Ru in the real system, and B3LYP/6-31G* and the Löwdin population are used.

a big difference in EA, it is then not strange that the electron prefers to be with dinitrobenzene—the electron acceptor in the model complex—which means $DNOA^-$ should be lower in energy than D^-NOA as found by constrained DFT.

Realizing that the discrepancy between our calculation results and the experimental results is probably not a weakness of DFT, we go back to check the model system that we chose. When we use the model system **2** to replace the real system **1** and put a negative charge on the model system, we neglect the positive hole on $Ru^{II}(tmbpy)_2$. While the actual charge distribution is hard to determine without a full scale calculation, its effect on the relative energy of the two locally charged states of the model system can be analyzed: with the positive fragment much closer to the donor than to the acceptor, it will bring down the energy of D^-NOA more than that of $DNOA^-$. To illustrate the effect, we simulate the positive fragment simply by putting a point charge at the location of Ru in the real system. The point charge is in the same plane as Mebpy and has a distance of 2.10 Å from both nitrogens in Mebpy. This choice is determined from the optimized geometry of $(tmbpy)_2Ru^{II}$-(Mebpy)-amH^+. Placing a whole charge of +1 would exaggerate the effect of the positive fragment and make D^-NOA lower in energy than $DNOA^-$ at all proton positions. A partial charge of +0.3 is found to give results in qualitative agreement with experiments (Figure 6). The point charge approach is no doubt a very crude simulation. Using a partial charge further makes the charge an ad hoc parameter. However, our purpose here is merely to demonstrate that, with an appropriate model system, constrained DFT generates qualitatively correct results.

From the results in Figure 6, the potential-energy difference (ΔG) between the D^-NOA state before proton transfer and the $DNOA^-$ state after proton transfer is about 5 kcal/mol, and the reaction barrier height is about 7 kcal/mol. Comparing Figure 6 with Figure 5a, one can see that the effect of the point charge is to vertically shift the two curves. Hence, the maximum possible barrier height and ΔG is about 13 kcal/mol (the minimum after proton transfer of the $DNOA^-$ curve has to be below the D^-NOA curve to make the reaction happen). It is known that DFT generally underestimates barrier heights[68,73−77] because DFT methods overstabilize the transition state because of greater self-interaction errors for systems of fractional charges than for systems of integer charges[66] (or, from an alternative point of view, because of the spurious buildup of nondynamical correlation[78]). In our calculations, however, we have largely reduced this effect by constraining the donor and the acceptor to have integer charges. Though some error still remains because the bridge charges are not constrained, we expect it to be small. Further, even without constraints, the B3LYP and B97-2 functionals have typical errors of about 5 and 3 kcal/mol, respectively, for barrier heights.[68] ΔG is calculated at equilibrium structures and has no known systematic errors for this type of system. Thus, we feel that the results in Figure 6 should be fairly accurate. Previous work[63] used multiconfiguration SCF (MCSCF) to study the same model system and found a much larger barrier height of 25 kcal/mol. However, the MCSCF calculation has only one electron in the active space, so it is effectively a Hartree−Fock (HF) calculation and does not include correlations. Hence, the lowering of the barrier height is probably due to the correlation effects that DFT methods account for. It is known that HF tends to overestimate barrier heights and needs correlations to lower them.[68] In this particular study, we note that this correlation-induced barrier lowering is *significant* and could potentially change our understanding of how PCET happens in this system.

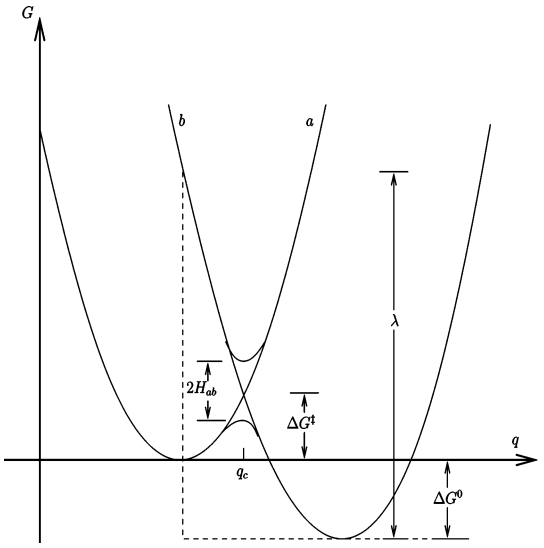

Figure 7. Picture of Marcus theory for electron-transfer reactions.

Conclusions

It has been shown that the direct optimization approach to constrained DFT can be generalized to include multiple constraints, where the constraint potentials are obtained efficiently within an expanded SCF calculation. When the proper Fock matrix is chosen, DIIS can be used to accelerate SCF convergence in a manner similar to that of usual DFT calculations, making constrained DFT truly efficient. Comparing different choices in defining the electron population of a molecule, we have found that the Löwdin population and the Becke weights population behave similarly and give nearly identical results for long-range charge-separated states. Generally, when the electron donor and acceptor have little density overlap, the constrained DFT results are well-defined. Hence, constrained DFT is naturally suited to long-range ET reactions. At short distances, the population scheme will be critical to the reliability of constrained DFT, and we will address this issue in future work.

To demonstrate the application of constrained DFT, we have done calculations on donor and acceptor molecular pairs that are separated far from each other and have shown that the energy of an infinitely separated CT state is equal to the energy sum of the donor and acceptor ionic states, as it should be. We have also studied a model system for the proton-coupled electron transfer in the donor−(amidinium−carboxylate)−acceptor complex. The potential-energy curves of the donor and acceptor states are generated using constrained DFT. With a partial point charge to simulate the positive fragment left out from the model system, we have obtained qualitative agreement with experimental results: the donor state is more stable before proton transfer, and the acceptor state is more stable after proton transfer. The barrier height is estimated to be 7 kcal/mol, which is significantly lower than the 25 kcal/mol barrier obtained with an uncorrelated MCSCF approach.

Before we close this report, we make the observation that the constrained potential-energy curves in the PCET case are actually *diabatic* curves, which implies that constrained DFT can fit well into Marcus theory[38,39] to describe electron-transfer reactions (Figure 7). Diabatic states *a* and *b*, which correspond to states before and after ET, are just two different constrained states. To make use of Marcus theory, however, requires locating the minimum energy point on each diabatic curve first. This means that one needs to be able to calculate the forces in constrained DFT and, therefore, perform geometry optimizations. Because of the variational nature of our method, it is not difficult to calculate the forces analytically in constrained DFT. We shall present an efficient computational scheme and its applications to electron-transfer systems in a future work.

As a final note, constrained DFT is not limited to electron-transfer calculations. By constraining the spin density instead of the total density, one can calculate exchange coupling constants in magnetic molecules.[79] There are other studies using constrained DFT on charge[29] and magnetization[30] fluctuations in solids, spin-dependent sticking of molecules on surfaces,[80] and parametrization of model Hamiltonians based on DFT calculations.[81] We expect our method to be useful for future applications in all of these areas.

Acknowledgment. We are grateful to Drs. Dreuw and Head-Gordon for providing us the ZnBC−BC complex structure. This work was made possible by a start-up grant from M. I. T.

Note Added after ASAP Publication. This article was released ASAP on March 15, 2006, with the incorrect Received Date. The correct version was posted on April 17, 2006.

References

(1) Hohenberg, P.; Kohn, W. *Phys. Rev.* **1964**, *136*, B864.

(2) Kohn, W.; Sham, L. *Phys. Rev.* **1965**, *140*, A1133.

(3) Runge, E.; Gross, E. K. U. *Phys. Rev. Lett.* **1984**, *52*, 997−1000.

(4) Casida, M. E. In *Recent Advances in Density Functional Methods, Part I*; Chong, D. P., Ed.; World Scientific: Singapore, 1995; pp 155−192.

(5) Petersilka, M.; Gossmann, U. J.; Gross, E. K. U. *Phys. Rev. Lett.* **1996**, *76*, 1212−1215.

(6) Bauernschmitt, R.; Ahlrichs, R. *Chem. Phys. Lett.* **1996**, *256*, 454−464.

(7) Hirata, S.; Head-Gordon, M. *Chem. Phys. Lett.* **1999**, *302*, 375−382.

(8) van Leeuwen, R.; Baerends, E. J. *Phys. Rev. A* **1994**, *49* (4), 2421−2431.

(9) Casida, M. E.; Jamorski, C.; Casida, K. C.; Salahub, D. R. *J. Chem. Phys.* **1998**, *108* (11), 4439−4449.

(10) Tozer, D. J. *Phys. Rev. A* **1998**, *58* (5), 3524−3527.

(11) Wu, Q.; Cohen, A. J.; Yang, W. *Mol. Phys.* **2005**, *103*, 711−717.

(12) Ayers, P.; Morrison, R.; Parr, R. *Mol. Phys.* **2005**, *103*, 2061−2072.

(13) Tozer, D. J.; Amos, R. D.; Handy, N. C.; Roos, B. O.; Serrano-Andres, L. *Mol. Phys.* **1999**, *97* (7), 859−868.

(14) Sobolewski, A. L.; Domcke, W. *Chem. Phys.* **2003**, *294* (1), 73−83.

(15) Fabian, J. *Theor. Chem. Acc.* **2001**, *106* (3), 199−217.

(16) Polıvka, T.; Sundström, V. *Chem. Rev.* **2004**, *104*, 2021−2071.

(17) Grätzel, M. *Nature* **2001**, *414*, 338−344.

(18) Mitschke, U.; Bäuerle, P. *J. Mater. Chem.* **2000**, *10*, 1471−1507.

(19) Tozer, D. J. *J. Chem. Phys.* **2003**, *119*, 12697.

(20) Dreuw, A.; Weisman, J. L.; Head-Gordon, M. *J. Chem. Phys.* **2003**, *119*, 2943−2946.

(21) Dreuw, A.; Head-Gordon, M. *J. Am. Chem. Soc.* **2004**, *126*, 4007−4016.

(22) Gritsenko, O. V.; Baerends, E. J. *J. Chem. Phys.* **2004**, *121* (2), 655−660.

(23) Tawada, Y.; Tsuneda, T.; Yanagisawa, S.; Yanai, T.; Hirao, K. *J. Chem. Phys.* **2004**, *120* (18), 8425−8433.

(24) Maitra, N. T. *J. Chem. Phys.* **2005**, *122* (23), 234104.

(25) Perdew, J. P.; Parr, R. G.; Levy, M.; Balduz, J. L., Jr. *Phys. Rev. Lett.* **1982**, *49*, 1691−1694.

(26) Wu, Q.; Van Voorhis, T. *Phys. Rev. A* **2005**, *72*, 024502.

(27) Dederichs, P. H.; Blügel, S.; Zeller, R.; Akai, H. *Phys. Rev. Lett.* **1984**, *53* (26), 2512−2515.

(28) Parr, R. G.; Yang, W. *Density-Functional Theory of Atoms and Molecules*; Oxford University Press: New York, 1989.

(29) Akai, H.; Blügel, S.; Zeller, R.; Dederichs, P. *Phys. Rev. Lett.* **1986**, *56* (22), 2407−2410.

(30) Zhang, Z.; Satpathy, S. *Phys. Rev. B* **1991**, *44* (24), 13319−13331.

(31) Cioslowski, J.; Stefanov, B. B. *J. Chem. Phys.* **1993**, *99* (7), 5151−5162.

(32) Prezhdo, O. V.; Kindt, J. T.; Tully, J. C. *J. Chem. Phys.* **1999**, *111* (17), 7818−7827.

(33) Talman, J. D.; Shadwick, W. F. *Phys. Rev. A* **1976**, *14*, 36−40.

(34) Yang, W.; Wu, Q. *Phys. Rev. Lett.* **2002**, *89*, 143002.

(35) Wu, Q.; Yang, W. *J. Chem. Phys.* **2003**, *118*, 2498−2509.

(36) Pan, X. Y.; Sahni, V.; Massa, L. *Phys. Rev. Lett.* **2004**, *93*, 130401.

(37) Pan, X. Y.; Sahni, V.; Massa, L. *Phys. Rev. A.* **2005**, *72*, 32505.

(38) Marcus, R. A. *Rev. Mod. Phys.* **1993**, *65*, 599−610.

(39) Barbara, P. F.; Meyer, T. J.; Ratner, M. A. *J. Phys. Chem.* **1996**, *100*, 13148−13168.

(40) High Performance Computational Chemistry Group. *NWChem, A Computational Chemistry Package for Parallel Computers*, version 4.6; Pacific Northwest National Laboratory: Richland, WA 99352, 2004.

(41) Press, W. H.; Teukolsky, S. A.; Vetterling, W. T.; Flannery, B. P. *Numerical Recipes*; Cambridge University Press: Cambridge, U. K., 1992.

(42) Pulay, P. *Chem. Phys. Lett.* **1980**, *73* (2), 393−398.

(43) Pulay, P. *J. Comput. Chem.* **1982**, *3* (4), 556−560.

(44) Parr, R. G.; Ayers, P. W.; Nalewajski, R. F. *J. Phys. Chem. A* **2005**, *109*, 3957−3959.

(45) Mulliken, R. S. *J. Chem. Phys.* **1955**, *23*, 1833−1840.

(46) Löwdin, P.-O. *J. Chem. Phys.* **1950**, *18* (3), 365−375.

(47) Becke, A. D. *J. Chem. Phys.* **1988**, *88* (4), 2547−2553.

(48) Becke, A. D. *J. Chem. Phys.* **1993**, *98* (7), 5648−5652.

(49) Lee, C.; Yang, W.; Parr, R. G. *Phys. Rev. B* **1988**, *37*, 785.

(50) Davidson, E. R. *J. Chem. Phys.* **1967**, *46* (9), 3320−3324.

(51) Clark, A. E.; Davidson, E. R. *Int. J. Quantum Chem.* **2003**, *93*, 384−394.

(52) Becke, A. D. *Phys. Rev. A* **1988**, *38*, 3098−3100.

(53) Wu, Q.; Ayers, P. W.; Yang, W. *J. Chem. Phys.* **2003**, *119*, 2978−2990.

(54) Ramirez, B. E.; Malmstrom, B. G.; Winkler, J. R.; Gray, H. B. *Proc. Natl. Acad. Sci. U.S.A.* **1995**, *92*, 11949.

(55) Brzezinski, P. *Biochemistry* **1996**, *35*, 5611.

(56) Berg, J. M. *Acc. Chem. Res.* **1995**, *28*, 14.

(57) Howell, E. E.; Villafranca, J. E.; Warren, M. S.; Oatley, S. J.; Kraut, J. *Science* **1986**, *231*, 1125.

(58) Crane, B. R.; Siegel, L. M.; Getzoff, E. D. *Science* **1995**, *270*, 59.

(59) Puglisi, J. D.; Chen, L.; Frankel, A. D.; Williamson, J. R. *Proc. Natl. Acad. Sci. U.S.A.* **1993**, *90*, 3680.

(60) Roberts, J. A.; Kirby, J. P.; Nocera, D. G. *J. Am. Chem. Soc.* **1995**, *117* (30), 8051−8052.

(61) Kirby, J. P.; Roberts, J. A.; Nocera, D. G. *J. Am. Chem. Soc.* **1997**, *119*, 9230−9236.

(62) Cukier, R. I.; Nocera, D. G. *Annu. Rev. Phys. Chem.* **1998**, *49*, 337−369.

(63) Soudackov, A.; Hammes-Schiffer, S. *J. Am. Chem. Soc.* **1999**, *121*, 10598−10607.

(64) Frisch, M. J.; Trucks, G. W.; Schlegel, H. B.; Scuseria, G. E.; Robb, M. A.; Cheeseman, J. R.; Montgomery, J. A., Jr.; Vreven, T.; Kudin, K. N.; Burant, J. C.; Millam, J. M.; Iyengar, S. S.; Tomasi, J.; Barone, V.; Mennucci, B.; Cossi, M.; Scalmani, G.; Rega, N.; Petersson, G. A.; Nakatsuji, H.; Hada, M.; Ehara, M.; Toyota, K.; Fukuda, R.; Hasegawa, J.; Ishida, M.; Nakajima, T.; Honda, Y.; Kitao, O.; Nakai, H.; Klene, M.; Li, X.; Knox, J. E.; Hratchian, H. P.; Cross, J. B.; Adamo, C.; Jaramillo, J.; Gomperts, R.; Stratmann, R. E.; Yazyev, O.; Austin, A. J.; Cammi, R.; Pomelli, C.; Ochterski, J. W.; Ayala, P. Y.; Morokuma, K.; Voth, G. A.; Salvador, P.; Dannenberg, J. J.; Zakrzewski, V. G.; Dapprich, S.; Daniels, A. D.; Strain, M. C.; Farkas, O.; Malick, D. K.; Rabuck, A. D.; Raghavachari, K.; Foresman, J. B.; Ortiz, J. V.; Cui, Q.; Baboul, A. G.; Clifford, S.; Cioslowski, J.; Stefanov, B. B.; Liu, G.; Liashenko, A.; Piskorz, P.; Komaromi, I.; Martin, R. L.; Fox, D. J.; Keith, T.; Al-Laham, M. A.; Peng, C. Y.; Nanayakkara, A.; Challacombe, M.; Gill, P. M. W.; Johnson, B.; Chen, W.; Wong, M. W.; Gonzalez, C.; Pople, J. A. *Gaussian 03*, revision B.05; Gaussian, Inc.: Pittsburgh, PA, 2003.

(65) Perdew, J. P.; Levy, M. *Phys. Rev. B* **1997**, *56*, 16021−16028.

(66) Zhang, Y.; Yang, W. *J. Chem. Phys.* **1998**, *109*, 2604−2608.

(67) Wilson, P. J.; Bradley, T. J.; Tozer, D. J. *J. Chem. Phys.* **2001**, *115*, 9233.

(68) Zhao, Y.; Pu, J.; Lynch, B. J.; Truhlar, D. G. *Phys. Chem. Chem. Phys.* **2004**, *6* (4), 673−676.

(69) *CRC Handbook of Chemistry and Physics 2001−2002*; CRC Press LLC: Boca Raton, FL, 2001.

(70) Galbraith, J. M.; Schaefer, H. F., III. *J. Chem. Phys.* **1996**, *105* (2), 862−864.

(71) Schumper, G. S.; Schaefer, H. F., III. *J. Chem. Phys.* **1997**, *107* (7), 2529−2541.

(72) de Oliveira, G.; Martin, J. M. L.; de Proft, F.; Geerlings, P. *Phys. Rev. A* **1999**, *60* (2), 1034−1045.

(73) Johnson, B. G.; Gonzales, C. A.; Gill, P. M.; Pople, J. A. *Chem. Phys. Lett.* **1994**, *221*, 100−108.

(74) Deng, L.; Branchadell, V.; Ziegler, T. *J. Am. Chem. Soc.* **1994**, *116*, 10645−10656.

(75) Baker, J.; Andzelm, J.; Muir, M.; Taylor, P. R. *Chem. Phys. Lett.* **1995**, *237*, 53.

(76) Hrouda, V.; Roeselova, M.; Bally, T. *J. Phys. Chem. A* **1997**, *101*, 3925−3935.

(77) Pu, J.; Truhlar, D. G. *J. Phys. Chem. A* **2005**, *109* (5), 773−778.

(78) Gritsenko, O. V.; Ensing, B.; Schipper, P. R. T.; Baerends, E. J. *J. Phys. Chem. A* **2000**, *104*, 8558−8565.

(79) Rudra, I.; Wu, Q.; Van Voorhis, T. *J. Chem. Phys.* **2006**, *124*, 024103.

(80) Behler, J.; Delley, B.; Lorenz, S.; Reuter, K. M. S. *Phys. Rev. Lett.* **2005**, *94* (3), 036104.

(81) Hybertsen, M. S.; Schluter, M.; Christensen, N. *Phys. Rev. B* **1989**, *39* (13), 9028−9041.

CT0503163